

LETTER TO THE EDITOR

The *Herschel* Virgo Cluster Survey: VII. Dust in cluster dwarf elliptical galaxies[★]

I. De Looze¹, M. Baes¹, S. Zibetti¹⁷, J. Fritz¹, L. Cortese⁷, J. I. Davies⁷, J. Verstacken¹, G. J. Bendo², S. Bianchi³, M. Clemens⁶, D. J. Bomans⁴, A. Boselli⁵, E. Corbelli³, A. Dariush⁷, S. di Serego Alighieri³, D. Fadda⁸, D. A. Garcia-Appadoo⁹, G. Gavazzi¹⁰, C. Giovanardi³, M. Grossi¹¹, T. M. Hughes⁷, L. K. Hunt³, A. P. Jones¹², S. Madden¹³, D. Pierini¹⁸, M. Pohlen⁷, S. Sabatini¹⁴, M. W. L. Smith⁷, C. Vlahakis¹⁵, and E. M. Xilouris¹⁶

(Affiliations can be found after the references)

March 30, 2022

ABSTRACT

We use the Science Demonstration Phase data of the *Herschel* Virgo Cluster Survey to search for dust emission of early-type dwarf galaxies in the central regions of the Virgo Cluster as an alternative way of identifying the interstellar medium. We present the first possible far-infrared detection of cluster early-type dwarf galaxies: VCC 781 and VCC 951 are detected at the 10σ level in the SPIRE 250 μm image. Both detected galaxies have dust masses of the order of $10^5 M_\odot$ and average dust temperatures $\approx 20\text{K}$. The detection rate (less than 1%) is quite high compared to the 1.7% detection rate for H α emission, considering that dwarfs in the central regions are more H α deficient. We conclude that the removal of interstellar dust from dwarf galaxies resulting from ram pressure stripping, harassment, or tidal effects must be as efficient as the removal of interstellar gas.

Key words. Galaxies: dwarf; Galaxies: individual: VCC 781; Galaxies: individual: VCC 951; Galaxies: ISM; ISM: dust, extinction

1. Introduction

Early-type dwarf galaxies (dEs) are the dominant morphological type in galaxy clusters. They were originally seen as a rather homogeneous population of dwarf galaxies with an old stellar age, no features resembling any recent or ongoing star formation, and no indications of a significant interstellar medium (ISM). This viewpoint has changed radically in the past few years. Deep imaging observations of dEs have revealed a heterogeneous morphology. In particular, the population of dEs can be subdivided into nucleated and non-nucleated subclasses and several papers report evidence of disks, spiral structure, bars or star formation (e.g., Jerjen et al. 2000; Barazza et al. 2002; Geha et al. 2003; Graham et al. 2003a,b; De Rijcke et al. 2003; Lisker et al. 2006a,b). Kinematical studies demonstrate that dEs are not simple pressure-supported systems: some dEs seem to be rotationally supported (Simien et al. 2002; Pedraz et al. 2002; Geha et al. 2003; De Rijcke et al. 2003; van Zee et al. 2004; Toloba et al. 2009), whereas others show evidence of kinematically decoupled cores (De Rijcke et al. 2004; Thomas et al. 2006).

Adding to this morphological and kinematical inhomogeneity is the detection of a significant interstellar medium in various dEs. Atomic and molecular gas was discovered for the first time in the Local Group dEs NGC 185 and NGC 205 using deep VLA and BIMA observations (Young & Lo 1997). In the Virgo cluster, Conselice et al. (2003) estimate a H α detection rate of 15% for dEs down to a 3σ limit of $8 \times 10^6 M_\odot$, while di Serego Alighieri et al. (2007) report a 1.7% H α detection rate with a 3σ detection limit of $3.5 \times 10^7 M_\odot$. Large amounts of cold interstellar matter are unexpected in dEs, as both internal (supernova

explosions) and external effects (ram-pressure stripping, galaxy interactions, tidal effects) are thought to be able to expel the gas from the shallow potential on short timescales (Michielsen et al. 2004; van Zee et al. 2004; Roediger & Hensler 2005; Boselli et al. 2008a,b; Valcke et al. 2008). That the H α detected dEs are found preferentially near the edge of the cluster supports the idea that understanding environmental effects is crucial to constraining the evolutionary history of dEs. Buyle et al. (2005) and Bouchard et al. (2005) performed H α observations in the outskirts of the Fornax cluster and the Sculptor group, respectively, and confirmed the tendency of gas-deficient galaxies to be located near the center of the cluster.

Continuum emission from interstellar dust is a promising alternative way to determine the ISM content of dEs. In particular, the ISM in the immediate surroundings of M87 can be traced by dust emission, as strong radio continuum emission considerably reduces the ALFALFA H α detection sensitivity within 1° of M87 (Giovannelli et al. 2007). To date, the Andromeda satellites NGC 205 and NGC 185 are the only dEs that have been detected in the far-infrared (Haas 1998; Marleau et al. 2006, 2009). In particular, no dust emission has been detected from cluster dEs. While extinction features in optical images are indicative of dust in at least some cluster dEs (Ferrarese et al. 2006; Lisker et al. 2006a,b), the direct detection of dust emission has been hampered by the limited resolution and sensitivity of the previous generation of far-infrared instrumentation. The advent of the *Herschel* Space Observatory (Pilbratt et al. 2010) offers new possibilities for mapping the ISM in dEs. In this paper, we report on our search for far-infrared emission from dEs in the Virgo Cluster, based on the Science Demonstration Phase (SDP) observations of the *Herschel* Virgo Cluster Survey (HeViCS¹). In Sect. 2, we describe the observations, data reduction, and sample

[★] *Herschel* is an ESA space observatory with science instruments provided by European-led Principal Investigator consortia and with important participation from NASA.

¹ More details on HeViCS can be found on <http://www.hevics.org>.

selection. In Sect. 3, we present our detections and in Sect. 4 we discuss the results of a stacking analysis of the non-detections. Sect. 5 gives our summary.

2. Observations and sample selection

The central 4×4 deg² region of the Virgo Cluster was observed by *Herschel* on 29 November 2009 as part of the HeViCS SDP observations. The observations were performed in parallel scan map mode, which means that both PACS (Poglitsch et al. 2010) and SPIRE (Griffin et al. 2010) data were collected. The scan speed was 60''/s and the field was covered in nominal and orthogonal directions to minimize $1/f$ noise. The PACS and SPIRE data were reduced with HIPE, with reduction scripts based on the standard reduction pipelines. For more details of the HeViCS SDP data reduction, we refer to Davies et al. (2010). We used the HeViCS SDP observations to search for dust emission from dEs in the central regions of the Virgo Cluster. Selecting the galaxies with morphological type dE and dS0 in the Goldmine catalogue (Gavazzi et al. 2003) resulted in an initial sample of 370 dEs. After the removal of 16 galaxies classified as background sources and the exclusion of 115 sources with an additional optical source within a 6'' radius, our final sample consisted of 239 dEs. Blind aperture photometry was applied to the PACS and SPIRE maps based on the positions of each of these 239 galaxies using Source Extractor (Bertin & Arnouts 1996).

3. Detected dEs

From this sample of 239 sources, 11 dEs were detected above 3σ in the SPIRE 250 μ m image. Nevertheless, we only report the clear detection of 2 dEs, VCC 781 and VCC 951, excluding all sources raising any kind of doubt. As such, VCC 1502 and VCC 788 were ruled out because their FIR location differs more than FWHM/2 from their optical position. VCC 832 was excluded because SDSS images detect a background source with substructure in the residual image, possibly indicating the presence of dust. Four other objects (VCC 752, VCC 815, VCC 1272, VCC 1512) fall within a crowded field of sources, enhancing the chances of their being background sources. For instance, Binggeli et al. (1985) reports the detection of a blue compact background galaxy, only 4'' to the west of the nucleus of VCC 815. Furthermore, VCC 752 and VCC 1272 appear to have SEDs that do not correspond to a single grey body. This failure in fitting a SED might either be caused by poor flux determination (the error bars are large compared to the low number of counts in the detection) or be a true indication that both detections originate in sources other than dEs. The other two sources VCC 1578 and VCC 767 are clearly detected in the SPIRE 250 μ m image at 4.8 and 4σ , respectively, but their high FIR flux relative to their faint optical appearance (both objects are low surface brightness [LSB] galaxies with B-band magnitudes of the order ~ 21 mag) aroused suspicion.

Dust has already been detected in LSBs (Hinz et al. 2007), but mainly in those with large amounts of star formation responsible for dust heating. A lack of evidence of recent star formation in VCC 767 and VCC 1578 strongly argues against the association of the 250 μ m emission with the corresponding dEs. Furthermore, we can identify a background source in the immediate surroundings of VCC 1578, which possibly contaminates the SPIRE 250 μ m emission.

Nonetheless, these questionable detections may still be caused by dust emission from dEs. Deeper fields in the future

might reveal dust emission in PACS images, where the higher spatial resolution may be able to rule out possible contamination by background sources.

On the other hand, VCC 781 and VCC 951 are detected unambiguously in the SPIRE 250 μ m image at 9.8 and 11.1σ , respectively (see Fig. 1). Adopting a fair 2σ detection cutoff in the other filters, VCC 781 is also detected in the PACS 100 μ m, PACS 160 μ m, SPIRE 350 μ m, and SPIRE 500 μ m bands. VCC 951 has additional detections only in both SPIRE 350 μ m and 500 μ m images. Unfortunately, it is impossible to measure fluxes for VCC 951 at 350 μ m and 500 μ m because VCC 951 and its neighbouring source, SDSS J122655.56+114000.5, are not resolved at these longer wavelengths.

Since the SPIRE 250 μ m image contains a vast number of sources, we need to address the possibility of false detections due to background sources. To perform this check accurately, we search all relevant images/catalogs (SDSS, Goldmine, 2MASS, UKIDSS, *Spitzer*) for sources within 18.1'' (FWHM of SPIRE 250 μ m) of the dwarf positions. For VCC 781, this identifies four SDSS sources within this PSF region that may be contaminating the dwarf emission. The superior resolution in the PACS 160 μ m image discards three of these optically identified objects, while the remaining source is rejected as a possible background candidate for the IR emission, based on the 24 μ m image (data from Fadda et al. in prep.), which has an even higher spatial resolution, and is clearly extended. Hence, the coincidence of the position of detections at various wavelengths makes us confident that the IR emission originates in VCC 781.

The SDSS DR7 catalog provides us with 5 detections within the PSF region of VCC 951, three of which are very likely to be artifacts in the source extraction, since we detected them in neither the SDSS nor the UKIDSS images during our visual inspection. The remaining two, morphologically classified as stellar-like objects, are located at distances of 8'' and 10'', and are also detected in the UKIDSS images. The 24 μ m image (see Fig. 1) shows some evidence of emission from both VCC 951 and one of the two aforementioned sources, which is spatially resolved at these wavelengths. Based on these data, we cannot definitely conclude that the IR emission detected by SPIRE comes from our dwarf galaxy, but deeper optical and NIR observations may help us to address the issue.

We conclude that, while our analysis is unable to definitely exclude a possible contamination from background sources, the weight of evidence is in favour of a true detection of dust in emission from dEs, and in particular from VCC 781.

These detected dEs have remarkable morphologies. Binggeli et al. (1985) classifies VCC 781 as dS0₃(5),N and VCC 951 as dS0(2),N or dE2 pec,N. These galaxies are also found by Lisker et al. (2006a) to harbor central substructures other than a disk, while Lisker et al. (2006b) identified blue central colors in VCC 781 and VCC 951. Figure 1 presents the $g-i$ color images in which VCC 781 and VCC 951, respectively, exhibit an obvious gradient in their radial $g-i$ color profiles, strengthening the assumption of recent star formation in the central regions (see also Lisker et al. 2006b).

According to the classification criterion ($3 < \text{FUV-H} < 6$) adopted in Boselli et al. (2008a), VCC 781 and VCC 951 can also be classified as possible transition objects. Although the FUV-H colours of 6.6 and 6.9 mag for VCC 781 and VCC 951, respectively, do not satisfy this relation, both galaxies are clearly located at the blue end of the dE galaxies in Boselli et al. (2008a). That SDSS nuclear spectra of both galaxies exhibit deep Hydrogen absorption lines ($\text{EW}[\text{H}\delta] > 4 \text{ \AA}$) indicates that they are in a post-starburst phase. This, and their 24 μ m emis-

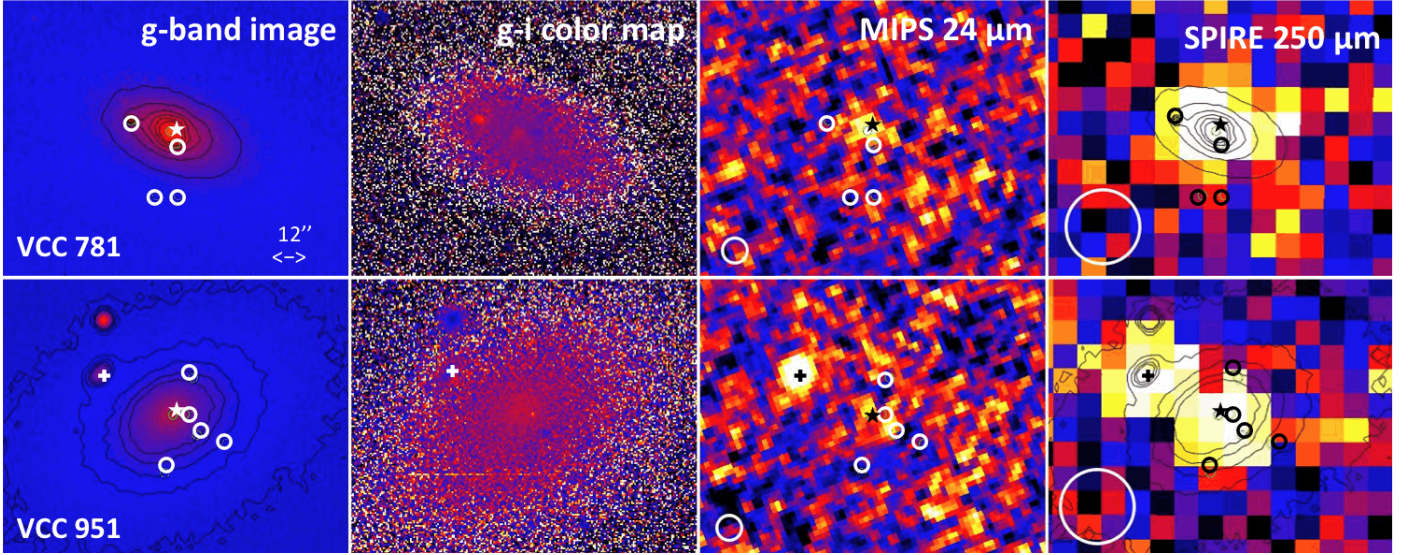


Fig. 1. All images are on the same scale. The FWHM of the beam is denoted in the MIPS 24 μm and SPIRE 250 μm images. g-band contours are overlaid on the SPIRE 250 μm image. The dwarf's position is indicated as a star, SDSS background sources as open circles, and the neighbouring source of VCC 951 as a cross.

sion, which is indeed centered on the optical nuclei and concentrated ($\sim 6''$ for VCC781 and point-like for VCC951), argues in favour of a connection between dust emission and a recent episode of star-formation.

To estimate the dust masses, we determined fluxes in bands where we had detections $> 2\sigma$. Initial apertures were fixed in the SPIRE 250 μm images based on the flattening of the growth curve. These apertures were subsequently adjusted to the pixel scale in other bands such that all apertures cover the same physical area. We first determined a representative dust temperature using the assumption that the dust is in thermal equilibrium with the interstellar radiation field. We used the Monte Carlo code SKIRT, which was initially developed to investigate the effects of dust extinction on the photometry and kinematics of galaxies (Baes et al. 2003), but evolved into a flexible tool that can model the absorption, scattering, and thermal emission of circumstellar discs and dusty galaxies (e.g. Vidal & Baes 2007; Baes et al. 2010). The stellar body of each galaxy was represented as an exponential profile, with parameters taken from the Goldmine database. The dust was assumed to have the same distribution as the stars. For the intrinsic SED of the model, we used the elliptical galaxy template SED from the PEGASE library (Fioc & Rocca-Volmerange 1997). Adding these ingredients, we find a representative dust equilibrium temperature of 20.7 K and 19.4 K for VCC 781 and VCC 951, respectively. Relying on these temperatures, we compute the dust masses according to

$$M_d = \frac{S_{250} D^2}{\kappa_{250} B_{250}(T_d)}, \quad (1)$$

where $D = 16.5$ Mpc is the distance to the Virgo Cluster (Mei et al. 2007), $\kappa_{250} = 0.4 \text{ m}^2 \text{ kg}^{-1}$ is the dust absorption coefficient (Draine & Li 2001), and $B_{250}(T_d)$ is the Planck function for the modeled temperature T_d . We obtain dust masses of $1.85 \times 10^5 M_\odot$ and $1.28 \times 10^5 M_\odot$ for VCC 781 and VCC 951, respectively.

As a check for consistency with datapoints other than the SPIRE 250 μm flux, we determine a second estimate of the temperature and dust mass based on grey body fitting. A single grey body fit to the 5 PACS and SPIRE fluxes gives $T_d = 19.5$ K and $M_d = 2.24 \times 10^5 M_\odot$ for VCC 781 (see Fig. 2). These results are

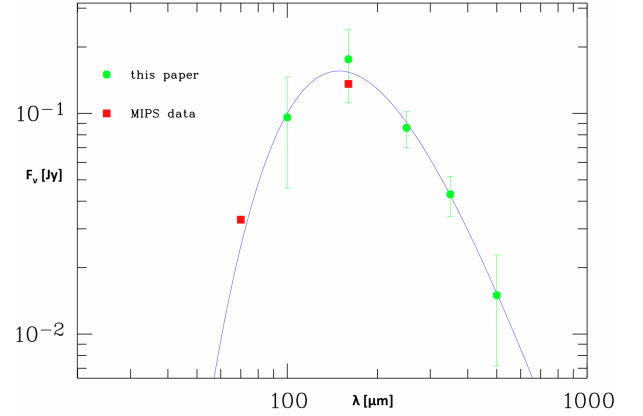


Fig. 2. The best-fitting grey body for VCC 781 with $T_d = 19.5$ K and dust mass $M_d = 2.24 \times 10^5 M_\odot$.

fully consistent with the temperature and dust mass of VCC 781 derived above. The MIPS 70 and 160 μm datapoints also satisfy the fitted greybody curve well (see Fig. 2).

Neither of the two dwarf galaxies is detected in H α . An H α mass upper limit was set to $2.3 \times 10^7 M_\odot$ for VCC 781 (Gavazzi et al. 2003) and $8.0 \times 10^6 M_\odot$ for VCC 951 (Conselice et al. 2003). Combining the estimated dust masses with these H α upper limits, and neglecting molecular gas, we find H α gas-to-dust upper limits of 124.3 and 62.5, respectively. These values are much lower than the expected canonical gas-to-dust ratio, possibly indicating that there is a dependence on other factors such as the metallicity and the environment.

4. Stacking analysis of non-detections

Apart from the two detections described in the previous section, we performed a stacking analysis of non-detected sources. In a first step we masked all bright sources in the surroundings of the dwarf galaxy (we prevented the inner pixel from being masked). We enlarged these masks using a boxcar with smoothing kernel of 3 pixels to cover the whole source. The final stacking al-

gorithm weighs the images with the inverse of the background variance to acquire the mean value in each pixel (of all unmasked pixels).

Stacking the SPIRE 250 μm images of all 227 non-detected early-type dwarf galaxies results in no detection. When taking apertures of size equal to the SPIRE 250 μm beam at random positions and calculating the standard deviation in their distribution, we derive an estimated background rms of 0.38 mJy. Assuming an average dust temperature of $T_d = 20\text{K}$, we convert this noise estimate to a 3σ dust mass detection limit of $M_d = 2.44 \times 10^3 M_\odot$.

Since the noise measured locally has an average value of rms = 5 mJy/beam, the stacking is not significantly affected by confusion noise (the rms almost scales as Gaussian noise, $5/\sqrt{227} = 0.33 \approx 0.38$). The complete survey of 4 cross-scans will reach a 1σ sensitivity of 4.72 mJy on small spatial scales, considering both instrumental and confusion noise (the latter is determined to be 4 mJy at SPIRE 250 μm). Assuming that the stacking procedure is only marginally affected by confusion noise, this value translates into a 3σ detection limit of $M_d = 2.0 \times 10^3 M_\odot$. Comparing both values, we conclude that the stacked image nearly reaches the sensitivity limit, as the detection limit will only improve by a factor of 1.2 after the complete survey.

5. Discussion and conclusion

We have reported on our search for far-infrared dust emission in a sample of 239 dEs at the centre of the Virgo Cluster. With a detection limit of about $10^4 M_\odot$, we have detected two objects at 10σ that have a high probability of being true detections of dEs. These two dwarf galaxies, VCC 781 and VCC 951, are the first detections of dust emission in dEs, apart from the Andromeda satellites NGC 205 and NGC 185. Applying a radiative transfer model to determine the equilibrium dust temperature in their interstellar radiation field, we determined temperatures of the order of 20 K in both galaxies. We estimate dust masses of the order $M_d = 10^5 M_\odot$ in both dEs.

In addition to independent detections of both atomic and molecular gas in dEs, the detection of dust emission here confirms the hypothesis that at least some dEs are transition objects gradually evolving from late-type to early-type, while falling into the cluster.

The detection of an interstellar dust medium in two dEs is rather unexpected, given the efficiency with which the ISM is removed from dwarf galaxies. Boselli et al. (2008a) found that gas removal by ram pressure stripping is extremely efficient in dwarfs galaxies, there being a decrease by ~ 2 orders of magnitude in ~ 150 Myr of time. In agreement with this rapid morphological transition, only a small number (10 – 16%) of dwarf galaxies exhibiting properties intermediate between star-forming and spheroidal galaxies are present in the Virgo Cluster.

di Serego Alighieri et al. (2007) find an H α detection rate in the Virgo cluster of only 1.7% to a 3σ mass limit $M_{H\alpha} = 3.5 \times 10^7 M_\odot$. Adopting a canonical gas-to-dust ratio of 1000 (which might still be a conservative lower limit as dEs in Virgo are expected to have metallicities significantly lower than observed in our own Milky Way), we recover a 3σ dust mass limit of $3.5 \times 10^4 M_\odot$, which is more or less the 3σ dust mass detection limit in the HeViCS SDP field. Our detection rate is also compatible with the 15% found by Conselice et al. (2003). Their H α upper limit corresponds to a 3σ dust mass limit of $8 \times 10^3 M_\odot$, well below the SDP detection limit. When also taking into account the position in the cluster, we consider our detection rate of less

than 1% surprisingly high. Indeed, H α detected dEs are preferentially located in the outskirts of the cluster and may not have been dramatically affected so far by the intracluster medium and interactions with other galaxies (Conselice et al. 2003; Buyle et al. 2005). di Serego Alighieri et al. (2007) also report that the majority of the detected H α -sources are located near the edges of the Virgo cluster. If gas and dust are tightly coupled and dust is as easily removed from the galaxy as gas by ram pressure stripping, harassment, or tidal effects, we expect that the dEs in the central regions of the Virgo Cluster will also be the most dust deficient. Clear evidence of efficient dust stripping in the Virgo Cluster is seen for the first time in H α -deficient spiral galaxies (Cortese et al. 2010). Future HeViCS observations will be able to provide an answer to this question – the HeViCS survey will not only go deeper (each field will be covered 4 times), but also wider (the total area covered will be $\sim 64 \text{ deg}^2$). A comparison of the far-infrared detection rate with the position in the cluster will tell us whether environmental effects have any influence on the detection rate.

References

- Baes, M., et al. 2003, MNRAS, 343, 1081
- Baes, M., Fritz, J., Gadotti, D. A. et al. 2010, A&A, this issue
- Barazza, F. D., Binggeli, B. & Jerjen, H. 2002, A&A, 391, 823
- Bertin, E., & Arnouts, S. 1996, A&AS, 117, 393
- Binggeli, B., Sandage, A., & Tammann, G. A. 1985, AJ, 90, 1681
- Boselli, A., Boissier, S., Cortese, L., & Gavazzi, G. 2008, ApJ, 674, 742
- Boselli, A., Boissier, S., Cortese, L., & Gavazzi, G. 2008, A&A, 489, 1015
- Bouchard, A., et al. 2005, AJ, 130, 2058
- Buyle, P. et al. 2005, MNRAS, 360, 853
- Conselice C. J. et al. 2003, ApJ, 591, 167
- Cortese, L., Davies, J. I., Pohlen, M. et al. 2010, A&A, this issue
- Davies, J. I., Baes, M., Bendo, G. J. et al. 2010, A&A, this issue
- De Rijcke, S. et al. 2003, A&A, 400, 119
- De Rijcke, S., Dejonghe, H., Zeilinger, W. W., & Hau, G. K. T. 2004, A&A, 426, 53
- di Serego Alighieri, S., et al. 2007, A&A, 474, 851
- Draine, B. T., & Li, A. 2001, ApJ, 551, 807
- Ferrarese, L. et al. 2006 ApJS, 164, 334
- Fioc, M., & Rocca-Volmerange, B. 1997, A&A, 326, 950
- Gavazzi G. et al. 2003, A&A, 400, 451
- Geha, M., Guhathakurta, P. & van der Marel, R. P. 2003, AJ, 126, 1794
- Giovanelli, R., et al. 2007, AJ, 133, 2569
- Graham, A. W. et al. 2003, AJ, 125, 2951
- Graham, A. W. & Guzman, R. 2003, AJ, 125, 2936
- Griffin, M., et al. 2010, A&A, this issue
- Haas, M. 1998, A&A, 337, L1
- Hinz, J. L., Rieke, M. J., Rieke, G. H., Willmer, C. N. A., Misselt, K., Engelbracht, C. W., Blaylock, M., & Pickering, T. E. 2007, ApJ, 663, 895
- Jerjen, H., Kalnajs, A., & Binggeli, B. 2000, A&A, 358, 845
- Lisker, T., Grebel, E. K., & Binggeli, B. 2006, AJ, 132, 497
- Lisker, T., et al. 2006, AJ, 132, 2432
- Marleau, F. R. et al. 2006, AJ, 646, 929
- Marleau, F. R., Noriega-Crespo, A. & Misselt, K. 2009, AAS, 214, 419.04, Bulletin of the American Astronomical Society, 41, 688
- Mei, S., et al. 2007, ApJ, 655, 144
- Michielsen, D., de Rijcke, S., & Dejonghe, H. 2004, Astronomische Nachrichten Supplement, 325, 122
- Pedraz, S. 2002, MNRAS, 332, L59
- Pilbratt, G., et al. 2010, A&A, this issue
- Poglitsch, A., et al. 2010, A&A, this issue
- Roediger, E., & Hensler, G. 2005, A&A, 433, 875
- Simien, F. & Prugniel, P. 2002, A&A, 384, 371
- Thomas, D., Brimiouille, F., Bender, R., Hopp, U., Greggio, L., Maraston, C., & Saglia, R. P. 2006, A&A, 445, L19
- Toloba, E., et al. 2009, ApJ, 707, L17
- Valcke, S., de Rijcke, S., & Dejonghe, H. 2008, MNRAS, 389, 1111
- van Zee, L., Skillman, E. D., & Haynes, M. P. 2004, AJ, 128, 121
- Vidal, E., & Baes, M. 2007, Baltic Astronomy, 16, 101
- Young, L. M., & Lo, K. Y. 1997, ApJ, 476, 127

- ¹ Sterrenkundig Observatorium, Universiteit Gent, Krijgslaan 281 S9, B-9000 Gent, Belgium
- ² Astrophysics Group, Imperial College London, Blackett Laboratory, Prince Consort Road, London SW7 2AZ, UK
- ³ INAF-Osservatorio Astrofisico di Arcetri, Largo Enrico Fermi 5, 50125 Firenze, Italy
- ⁴ Astronomical Institute, Ruhr-University Bochum, Universitaetsstr. 150, 44780 Bochum, Germany
- ⁵ Laboratoire d'Astrophysique de Marseille, UMR 6110 CNRS, 38 rue F. Joliot-Curie, F-13388 Marseille, France
- ⁶ INAF-Osservatorio Astronomico di Padova, Vicolo dell'Osservatorio 5, 35122 Padova, Italy
- ⁷ Department of Physics and Astronomy, Cardiff University, The Parade, Cardiff, CF24 3AA, UK
- ⁸ NASA *Herschel* Science Center, California Institute of Technology, MS 100-22, Pasadena, CA 91125, USA
- ⁹ European Southern Observatory, Alonso de Cordova 3107, Vitacura, Santiago, Chile
- ¹⁰ Università di Milano-Bicocca, piazza della Scienza 3, 20100, Milano, Italy
- ¹¹ CAAUL, Observatório Astronómico de Lisboa, Universidade de Lisboa, Tapada da Ajuda, 1349-018, Lisboa, Portugal
- ¹² Institut d'Astrophysique Spatiale (IAS), Batiment 121, Université Paris-Sud 11 and CNRS, F-91405 Orsay, France
- ¹³ Laboratoire AIM, CEA/DSM- CNRS - Université Paris Diderot, Irfu/Service d'Astrophysique, 91191 Gif sur Yvette, France
- ¹⁴ INAF-Istituto di Astrofisica Spaziale e Fisica Cosmica, via Fosso del Cavaliere 100, I-00133, Roma, Italy
- ¹⁵ Leiden Observatory, Leiden University, P.O. Box 9513, NL-2300 RA Leiden, The Netherlands
- ¹⁶ National Observatory of Athens, I. Metaxa and Vas. Pavlou, P. Penteli, GR-15236 Athens, Greece
- ¹⁷ Max-Planck-Institut fuer Astronomie, Koenigstuhl 17, D-69117 Heidelberg, Germany
- ¹⁸ Max-Planck-Institut fuer extraterrestrische Physik, Giessenbachstrasse, 85748 Garching, Germany